

# Analysis of interface electronic structure in $\text{In}_x\text{Ga}_{1-x}\text{N}/\text{GaN}$ heterostructures

H. Zhang, E. J. Miller, and E. T. Yu<sup>a)</sup>

*Department of Electrical and Computer Engineering, University of California at San Diego, La Jolla, California 92093-0407*

C. Poblenz and J. S. Speck

*Materials Department, University of California at Santa Barbara, Santa Barbara, California 93106*

(Received 18 January 2004; accepted 9 March 2004; published 20 August 2004)

Capacitance–voltage profiling was used to measure interfacial polarization charge densities and conduction-band offsets at  $\text{In}_x\text{Ga}_{1-x}\text{N}/\text{GaN}$  heterojunction interfaces for  $x=0.054$  and  $0.09$ . A variant of the conventional analysis technique used to deduce interface charge density and band-offset values from capacitance–voltage data was developed and applied. Conduction-band offsets of  $0.09\pm 0.07$  and  $0.22\pm 0.05$  eV are obtained for  $x=0.054$  and  $0.09$ , respectively. Polarization charge densities derived from these measurements are  $(1.80\pm 0.32)\times 10^{12}$  and  $(4.38\pm 0.36)\times 10^{12}$  e/cm<sup>2</sup> for  $x=0.054$  and  $0.09$ , respectively. These values are somewhat lower than those predicted theoretically, but are in good agreement with values inferred from a substantial body of optical data reported for  $\text{In}_x\text{Ga}_{1-x}\text{N}/\text{GaN}$  quantum-well structures. © 2004 American Vacuum Society. [DOI: 10.1116/1.1768190]

## I. INTRODUCTION

$\text{In}_x\text{Ga}_{1-x}\text{N}/\text{GaN}$  heterostructures are of outstanding current interest for both electronic<sup>1,2</sup> and optoelectronic<sup>3</sup> device applications. The design, analysis, and optimization of such devices require a detailed, quantitatively accurate understanding of electronic structure at the  $\text{In}_x\text{Ga}_{1-x}\text{N}/\text{GaN}$  heterojunction interface, and in particular requires accurate knowledge of parameters such as the interfacial polarization charge densities and the conduction- and valence-band offsets. However, the measurement of polarization fields and charge densities is often complicated by the influence of free-carrier screening effects, and the experimental determination of band offsets is fraught with a variety of experimental and modeling perils that can lead to inaccurate or highly uncertain results.

In this study, we have used capacitance–voltage ( $C-V$ ) profiling through  $\text{In}_x\text{Ga}_{1-x}\text{N}/\text{GaN}$  heterojunction interfaces to measure both interfacial polarization charge densities and conduction band offsets for heterojunctions with  $x=0.054$  and  $0.09$ . Our results yield a conduction- to valence-band offset ratio  $\Delta E_C:\Delta E_V=58:42$  in this range of compositions, and polarization charge densities of  $(1.80\pm 0.32)\times 10^{12}$  and  $(4.38\pm 0.36)\times 10^{12}$  e/cm<sup>2</sup>, respectively—somewhat lower than theoretical predicted values but consistent with results inferred from several optical experiments reported with literature. We have also developed and applied a variant of the conventional analysis technique used to derive interfacial charge density and band-offset values from  $C-V$  profiling data that substantially reduces susceptibility to noise and, hence, allows more straightforward and reliable extraction of these parameters.

## II. EXPERIMENT

The epitaxial layer structure of the  $\text{In}_x\text{Ga}_{1-x}\text{N}/\text{GaN}$  samples used in this study is shown schematically in Fig. 1. Two samples were characterized: one with a 50 nm  $\text{In}_{0.09}\text{Ga}_{0.91}\text{N}$  layer and the other with a 30 nm  $\text{In}_{0.054}\text{Ga}_{0.946}\text{N}$  layer. The epitaxial layer structures employed layer thicknesses and dopant concentrations designed to ensure that undepleted regions with negligibly small electric field were present above and below each heterojunction interface. To achieve this,  $n$ -type doping of  $\sim 10^{18}$  cm<sup>-3</sup> in the  $\text{In}_x\text{Ga}_{1-x}\text{N}$  layer and the surrounding GaN layers shown in Fig. 1 was targeted. These regions are required to ensure proper analysis of the  $C-V$  spectra for determination of interface charge densities and band offsets. Both samples were grown by rf-plasma assisted molecular beam epitaxy (MBE) on a  $\sim 1.5$   $\mu\text{m}$  thick metalorganic chemical vapor deposition GaN template deposited on a sapphire substrate.<sup>4</sup> The MBE epitaxial layers were grown at 650 °C and the crystal polarity was determined to be Ga face, based on cross-sectional transmission electron microscope and atomic force microscope measurements. X-ray reciprocal space mapping measurements were used to determine the composition of the  $\text{In}_x\text{Ga}_{1-x}\text{N}$  layers and to confirm that the heterostructures were fully strained.

The prerequisite of the  $C-V$  profiling method is the steady-state condition, and the incremental charge assumption underlying this technique is rigorously justified only if there is zero or negligible current flow in the device under dc bias.<sup>5</sup> This requirement can be problematic for nitride semiconductor material grown by MBE, for which leakage currents in Schottky contacts can be very high.<sup>6,7</sup> For the  $\text{GaN}/\text{In}_{0.09}\text{Ga}_{0.91}\text{N}/\text{GaN}$  sample, a thin layer of silicon oxide (30–130 Å) was deposited on the  $\text{In}_{0.09}\text{Ga}_{0.91}\text{N}$  sample by plasma-enhanced chemical vapor deposition (PECVD) to reduce the current density from several hundred A per square centimeter to approximately 10 A per square centimeter. A

<sup>a)</sup>Electronic mail: ety@ece.ucsd.edu

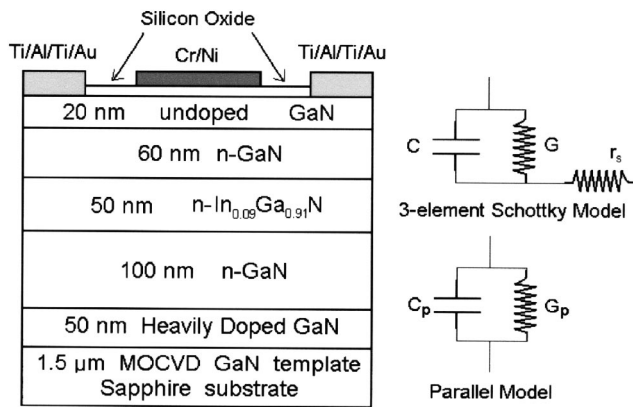


FIG. 1. Schematic diagram of the  $\text{In}_x\text{Ga}_{1-x}\text{N}/\text{GaN}$  epitaxial layer structure and the corresponding equivalent circuit models used in this study.

preparatory surface treatment<sup>8</sup> was required to reduce the oxide–GaN interface state density. The specific procedure employed was as follows: the sample was first cleaned in the supersonic agitated organic solvents (TCE, acetone, isopropanol alcohol, and methanol) and then soaked in an  $\text{NH}_4\text{OH}$  solution at  $50^\circ\text{C}$  for 15 min. After each step, the sample was thoroughly rinsed in deionized water. An  $\text{N}_2$  plasma treatment was performed at  $300^\circ\text{C}$  with an excitation power of 30 W for 5 min. The oxide was then immediately deposited in the same chamber at a lower temperature to avoid contamination. The deposited oxide thus reduced the reverse-bias leakage current by 1–2 orders of magnitude, which was sufficient for these measurements. The combination of a very thin oxide layer with the plasma and chemical surface treatment prior to oxide deposition allowed us to avoid hysteresis effects associated with interface states in our  $C$ – $V$  measurement. Numerical simulations were used to confirm that the effect of the oxide layer on the potential drop across the semiconductor depletion layer was not significant. Optical lithography was used to define the ohmic contact region, within which the PECVD-grown oxide was removed using buffered oxide etch before ohmic metal deposition. Ti/Al/Ti/Au (330 Å/770 Å/300 Å/1000 Å) ohmic contact metallization was deposited using electron beam evaporation and then annealed in forming gas at  $650^\circ\text{C}$  for 1 min. Cr/Ni (200 Å/1200 Å) metallization was then used for the Schottky contact with Cr serving to enhance the adhesion of Ni to the oxide layer. For the  $\text{In}_{0.054}\text{Ga}_{0.946}\text{N}$  sample, the leakage current density is about  $150\text{ A}/\text{cm}^2$ , small enough to allow accurate  $C$ – $V$  characterization, and therefore no oxide was deposited. 1500 Å thick Ni was directly evaporated on the sample surface to form the Schottky contact with Ti/Al/Ti/Au metallization used to form the ohmic contact as described above.

Capacitance–voltage measurements were performed using an HP 4285A Precision  $LCR$  meter at frequencies ranging from 100 kHz to 1 MHz, at room temperature under ambient lighting conditions using the parallel circuit mode of the HP4285A. The presence of the insulating oxide layer in one diode structure as described above leads to a high series re-

sistance, which must be properly accounted for in the analysis of  $C$ – $V$  spectra. As shown in Fig. 1, a three-element circuit incorporating the depletion capacitance  $C$ , conductance  $G$ , and a parametric series resistance  $r_s$  is used to model the behavior of the Schottky diode.  $r_s$  is assumed to include the resistance of the undepleted bulk material, contacts, and insulating oxide layer. Measurements were obtained in the parallel mode of operation of the HP4285A, and therefore yielded capacitance  $C_p$  and conductance  $G_p$ . A simple circuit analysis yields the following relationships<sup>9</sup> among  $C_p$ ,  $G_p$ ,  $C$ ,  $G$ ,  $r_s$  and the measurement angular frequency  $\omega$ :

$$C_p = \frac{C}{(1 + r_s G)^2 + (\omega r_s C)^2}, \quad (1)$$

$$G_p = \frac{G(1 + r_s G) + r_s (\omega C)^2}{(1 + r_s G)^2 + (\omega r_s C)^2}. \quad (2)$$

As is evident from Eqs. (1) and (2), the measured capacitance and conductance,  $C_p$  and  $G_p$ , respectively, can exhibit substantial frequency dependence and can deviate significantly from the actual capacitance and conductance of interest when  $r_s$  is large compared to  $1/G$  or  $1/\omega C$ . Analysis of and correction for these effects of series resistance were therefore essential in our investigation.

The series resistance  $r_s$  was assumed to be constant and was determined from the measured conductance  $G_p$  under forward bias. For sufficiently large forward bias,  $G$  becomes large compared to  $\omega C$  and  $1/r_s$ , and Eq. (2) can be written approximately as

$$\frac{1}{G_p} \approx \frac{1}{G} + r_s \approx r_s. \quad (3)$$

Once  $r_s$  was determined in this manner,  $C$  and  $G$  were obtained from the measured values of  $G_p$  and  $C_p$  using Eqs. (1) and (2). Figure 2 shows measured capacitances  $C_p$  for each sample structure at selected frequencies ranging from 100 kHz to 1 MHz. The frequency-dependent characteristic of  $C_p$  is especially obvious under small forward bias when  $r_s$  is much larger than  $1/G$ . After the correction for series resistance effects, this frequency dependence disappears and the corrected  $C$ – $V$  curves, also shown in Fig. 2, can be more directly associated with the properties of the semiconductor heterostructure under investigation. There remains a dependence of the  $C$ – $V$  curves on frequency at large negative bias voltage, possibly due to interface states at the  $\text{GaN}/\text{In}_x\text{Ga}_{1-x}\text{N}$  heterojunction. At higher frequencies, trapped charges at the interface may not be modulated and therefore the capacitance is lower than that obtained at lower frequencies. However, the frequency dependence of the capacitance at these voltages has only a very small effect on the determination of the interface polarization charge density and conduction-band offset, described in Sec. III. The series resistance correction has a substantial influence in determining the carrier concentration near the surface of the diodes, particularly in the  $\text{GaN}/\text{In}_{0.09}\text{Ga}_{0.91}\text{N}/\text{GaN}$  sample, which has a much larger series resistance  $r_s$  because of the oxide layer,

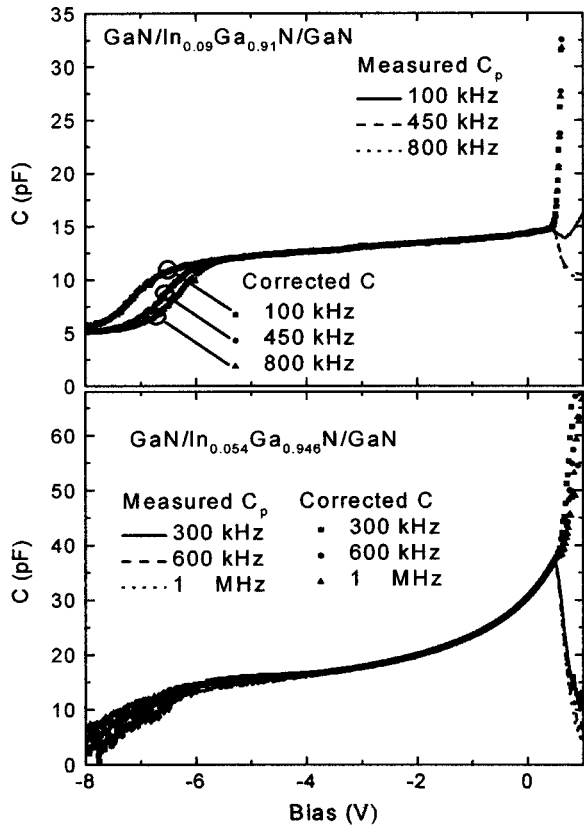


FIG. 2. Measured  $C_p$  and the derived capacitance after the consideration of the series resistance effect for  $\text{GaN}/\text{In}_{0.09}\text{Ga}_{0.91}\text{N}/\text{GaN}$  (top) and for  $\text{GaN}/\text{In}_{0.054}\text{Ga}_{0.946}\text{N}/\text{GaN}$  (bottom).

but has a relatively minor effect in determining the carrier concentration farther below the surface. Values for  $r_s$  ranged from 50–80  $\Omega$  for the  $\text{GaN}/\text{In}_{0.054}\text{Ga}_{0.946}\text{N}/\text{GaN}$  sample to 1200–1300  $\Omega$  for the  $\text{GaN}/\text{In}_{0.09}\text{Ga}_{0.91}\text{N}/\text{GaN}$  sample.

### III. RESULTS AND DISCUSSION

The apparent carrier distribution  $n^*$  and depletion depth  $w$  are given by<sup>9</sup>

$$n^* = -\frac{2}{q\varepsilon S^2 d(1/C^2)/dV}, \quad (4)$$

$$w = \frac{\varepsilon_1 S}{C} \quad \text{if } w < w_h,$$

$$w = \frac{\varepsilon_2 S}{C} + \left(1 - \frac{\varepsilon_2}{\varepsilon_1}\right) w_h \quad \text{if } w > w_h, \quad (5)$$

where  $q$  is the electronic charge,  $\varepsilon_1$  and  $\varepsilon_2$  are the dielectric constants of the semiconductor materials in the upper and lower layers, respectively,  $S$  is the area under the Schottky contact, and  $w_h$  is the heterojunction position. Figure 3 shows apparent carrier concentration profiles computed using Eqs. (4) and (5) for both heterostructure structures employed in these studies. Electron accumulation at the upper  $\text{GaN}/\text{In}_x\text{Ga}_{1-x}\text{N}$  interfaces is clearly evident, and the carrier concentration profiles determined in this manner are seen to be very consistent for frequencies ranging from 100 kHz to 1

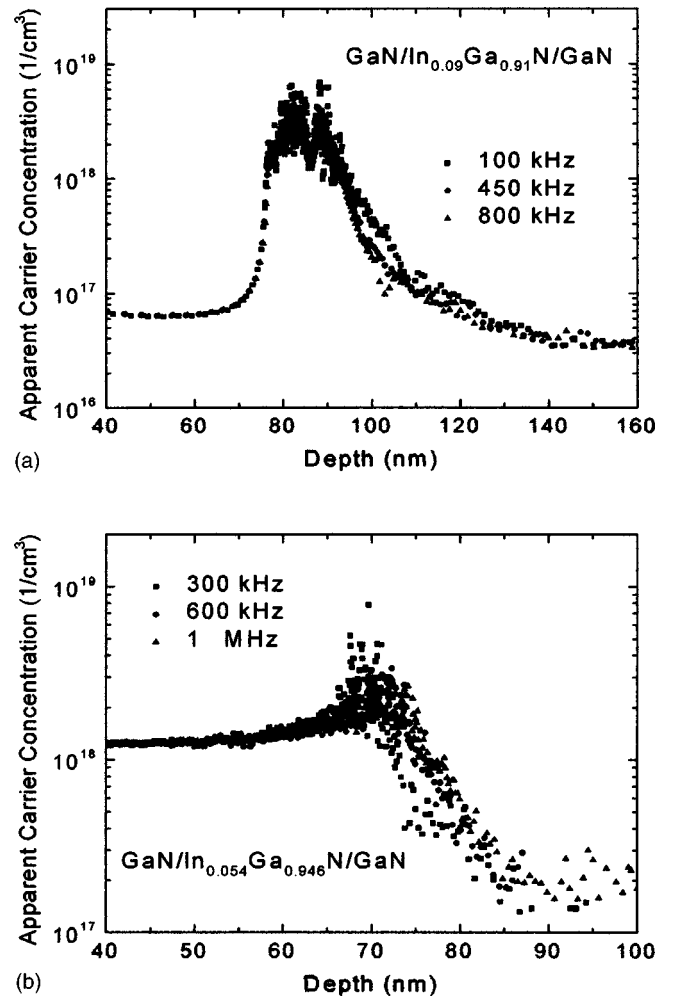


FIG. 3. Apparent carrier concentration profiles: (a) for the  $\text{In}_{0.09}\text{Ga}_{0.91}\text{N}/\text{GaN}$  heterostructure, derived from  $C-V$  data obtained at frequencies of 100 kHz ( $\blacksquare$ ), 450 kHz ( $\blacklozenge$ ), and 800 kHz ( $\blacktriangle$ ) (top) and (b) for the  $\text{In}_{0.054}\text{Ga}_{0.946}\text{N}/\text{GaN}$  heterostructure, derived from  $C-V$  data obtained at frequencies of 300 kHz ( $\blacksquare$ ), 600 kHz ( $\blacklozenge$ ), and 1 MHz ( $\blacktriangle$ ) (bottom).

MHz, although the background dopant concentrations obtained are generally somewhat lower than targeted. The scatter in the apparent carrier concentration profile is due primarily to noise in the  $C-V$  data, which is magnified in the profile of  $n^*$  due to the need to numerically differentiate the  $C-V$  profile. However, this scatter has little effect on the subsequent determination of  $Q_i$  and  $\Delta E_C$ . The origin of the dip that appears within the concentration peak in Fig. 3(a) is not certain, but may be related to the occupation if multiple quantum confined states are at the  $\text{GaN}/\text{In}_{0.09}\text{Ga}_{0.91}\text{N}$  interface. Solutions of Poisson and Schrödinger equations for this structure suggest that more than one quantum-confined state may be occupied, leading to an electron concentration profile such as that shown in Fig. 3(a).

Once the apparent carrier concentration profile has been determined, the interface charge density  $Q_i$  and the conduction band offset  $\Delta E_C$  at the heterojunction interface are given by<sup>10</sup>

$$Q_i = q \int_{w_1}^{w_2} (n^*(w) - N_d^+(w)) dw, \quad (6)$$

$$\Delta E_C = -q^2 \int_{w_1}^{w_2} \left\{ \frac{1}{\varepsilon(w)} [N_d^+(w) - n^*(w)] (w - w_h) \right\} dw - kT \left[ \ln \left( \frac{n_1/N_{C1}}{n_2/N_{C2}} \right) + \frac{1}{\sqrt{8}} \left( \frac{n_1}{N_{C1}} - \frac{n_2}{N_{C2}} \right) \right], \quad (7)$$

where  $N_d^+(w)$  is the ionized donor concentration at depth  $w$  below the metal–semiconductor interface,  $N_{C1}$  and  $N_{C2}$  are the conduction-band effective densities of states of the first and second layer of semiconductor material, respectively, and  $n_1$  and  $n_2$  are the free electron concentrations in the corresponding layers. The integration limits  $w_1$  and  $w_2$  are chosen to be far from the heterojunction, where the electric field is negligible. The physical meaning of these two equations is self-evident. Equation (6) is the integration of the carrier and donor charges near the heterojunction. Due to the charge neutrality condition, integration of these charges yields the fixed charge at the heterointerface, which for nitride heterojunction interfaces we assume to be dominated by the polarization charge. The first part of Eq. (7) is the first moment of the carrier and donor charges, and gives the total built-in potential within these two layers. The second part of Eq. (7) accounts for the Fermi-level variations in each layer, with the combination of these two terms yielding the conduction band offset  $\Delta E_C$ .

While this approach allows, in principle, straightforward determination of  $Q_i$  and  $\Delta E_C$  from capacitance–voltage spectra, the accurate construction of the apparent carrier concentration profile  $n^*(w)$  typically requires considerable care as a numerical differentiation of the capacitance–voltage curve must be performed. This differentiation can magnify any noise present in the capacitance data, potentially leading to inaccuracies or at least increased uncertainty in  $n^*(w)$ ,  $Q_i$ , and  $\Delta E_C$ . An alternate approach that largely circumvents these difficulties can be derived by noting that, from Eq. (5),  $dw = -(\varepsilon_1 S / C^2) dC$ . Using this relationship, Eqs. (6) and (7) can be transformed with  $Q_i$  and  $\Delta E_C$  thereby given by

$$Q_i = \frac{1}{S} \int_{V_1}^{V_2} C dV - q [n_1(w_h - w_1) + n_2(w_2 - w_h)], \quad (8)$$

$$\Delta E_C = -q^2 \left[ \frac{1}{2\varepsilon_2} n_2(w_2 - w_h)^2 - \frac{1}{2\varepsilon_1} n_1(w_h - w_1)^2 \right] + q \left[ V_2 - V_1 - \frac{w_h}{\varepsilon_1 S} \int_{V_1}^{V_2} C dV \right] - kT \left[ \ln \left( \frac{n_1/N_{C1}}{n_2/N_{C2}} \right) + \frac{1}{\sqrt{8}} \left( \frac{n_1}{N_{C1}} - \frac{n_2}{N_{C2}} \right) \right], \quad (9)$$

where  $V_1$  and  $V_2$  are the voltages at which the depletion layer width reaches  $w_1$  and  $w_2$ , respectively. From Eqs. (8) and (9) we see that the apparent carrier concentration profile  $n^*(w)$  plays only an intermediary role mathematically in the

determination of  $Q_i$  and  $\Delta E_C$ , which can be obtained by direct integration of the capacitance–voltage curve. This approach allows numerical challenges associated with the computation of  $d(1/C^2)/dV$  to be avoided, and enables a more straightforward and robust calculation of  $Q_i$  and  $\Delta E_C$ . We have used both Eqs. (4)–(7) and (8)–(9) to calculate polarization charge densities and conduction band offsets, and with proper care using the former approach, both computations yield very consistent results.

By analyzing data acquired at measurement frequencies varying from 100 kHz to 1 MHz, and obtained from several different diodes, we have determined the conduction band offsets to be  $\Delta E_C = 0.09 \pm 0.07$  and  $\Delta E_C = 0.22 \pm 0.05$  eV for the  $\text{GaN}/\text{In}_x\text{Ga}_{1-x}\text{N}$  heterojunction with  $x = 0.054$  and  $0.09$ , respectively. The uncertainty in  $\Delta E_C$  for  $x = 0.054$  sample is relatively large, partly due to the small value of the conduction band offset itself at this composition. Using energy band gaps of 3.42 eV for GaN, 3.225 eV for  $\text{In}_{0.054}\text{Ga}_{0.946}\text{N}$ , and 3.06 eV for  $\text{In}_{0.09}\text{Ga}_{0.91}\text{N}$ ,<sup>11,12</sup> coherently strained to GaN, and based on the relative uncertainties in our measured conduction-band offsets, we compute a weighted average of the band offset ratio  $\Delta E_C : \Delta E_V$  and obtain  $\Delta E_C : \Delta E_V = 58:42$ . In comparison, an analysis of deep yellow photoluminescence<sup>13</sup> in GaN and  $\text{In}_x\text{Ga}_{1-x}\text{N}$  alloys yielded a conduction-to-valence band offset ratio of 62:38 for  $x \leq 0.14$ , corresponding to  $\Delta E_C = 0.11$  and  $\Delta E_C = 0.18$  eV for the  $\text{In}_{0.054}\text{Ga}_{0.946}\text{N}/\text{GaN}$  and  $\text{In}_{0.09}\text{Ga}_{0.91}\text{N}/\text{GaN}$  interfaces, respectively. This approach assumes the existence of a shallow donor level that follows the conduction band edge and a pinned deep acceptor level that maintains a constant absolute energy in the  $\text{In}_x\text{Ga}_{1-x}\text{N}$  and GaN systems; determination of the corresponding luminescence energy as a function of composition in  $\text{In}_x\text{Ga}_{1-x}\text{N}$  alloys therefore allows the absolute conduction-band edge energy, and consequently conduction-band offsets, to be deduced. X-ray photoemission spectroscopy has yielded<sup>14,15</sup> a valence-band offset for the  $\text{InN}/\text{GaN}$  heterojunction of 1.05 eV, which in Ref. 1 is taken to imply a ratio  $\Delta E_C : \Delta E_V = 63:37$ . The conduction-band offsets corresponding to this ratio are 0.13 and 0.21 eV for  $x = 0.054$  and  $x = 0.09$ , respectively. A capacitance–voltage analysis<sup>16</sup> of a  $p\text{-In}_x\text{Ga}_{1-x}\text{N}/n\text{-GaN}$  diode to obtain the valence-band offset  $\Delta E_V$  implies values for  $\Delta E_C$  of 0.13 and 0.22 eV for the  $\text{In}_{0.054}\text{Ga}_{0.946}\text{N}$  and  $\text{In}_{0.09}\text{Ga}_{0.91}\text{N}/\text{GaN}$  interfaces, respectively. Thus, we see that the conduction-band offsets obtained from these different experiments, as summarized in Fig. 4, show very good consistency and all the results fall within the range of measurement uncertainty of this work.

The polarization charge densities at the  $\text{In}_{0.054}\text{Ga}_{0.946}\text{N}/\text{GaN}$  and  $\text{In}_{0.09}\text{Ga}_{0.91}\text{N}/\text{GaN}$  interfaces deduced from our measurements are  $(1.80 \pm 0.32) \times 10^{12}$  and  $(4.38 \pm 0.36) \times 10^{12}$   $e/\text{cm}^2$ , respectively. In comparison, theoretical calculations yield substantially higher values, ranging from  $4.43 \times 10^{12}$  to  $5.25 \times 10^{12}$   $e/\text{cm}^2$  for  $x = 0.054$  and from  $6.84 \times 10^{12}$  to  $8.74 \times 10^{12}$   $e/\text{cm}^2$  for  $x = 0.09$ , depending on the different elastic, piezoelectric, and lattice constants assumed.<sup>17</sup> Although few direct measurements of the  $\text{In}_x\text{Ga}_{1-x}\text{N}/\text{GaN}$  interface polarization charge densities are

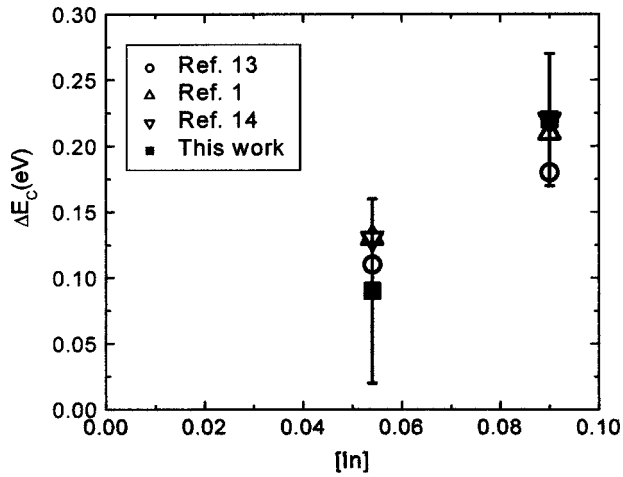


FIG. 4. Reported values and our measured values for  $\Delta E_C$  for the  $\text{In}_x\text{Ga}_{1-x}\text{N}/\text{GaN}$  heterojunction.

readily available, polarization charge densities can be inferred from values of the electric field magnitude within  $\text{In}_x\text{Ga}_{1-x}\text{N}/\text{GaN}$  quantum-well structures deduced from photoluminescence,<sup>18–21</sup> electroabsorption,<sup>22</sup> and electrotransmission<sup>23</sup> experiments. Because of the polarization charges present at each heterojunction interface, a large internal electric field is induced within an  $\text{In}_x\text{Ga}_{1-x}\text{N}/\text{GaN}$  quantum well. Due to carrier screening effects, however, determination of the polarization charge density corresponding to a reported value for the electric field requires a self-consistent solution of the Poisson–Schrödinger equations for the full quantum well structure. Thus, by assuming the quantum-well structure to be known *a priori* and taking the polarization charge density at the heterojunction interface as a variable parameter, we have used a one-dimensional Poisson/Schrödinger solver<sup>24</sup> to compute the corresponding electric field, as shown in Fig. 5 for the multiple-quantum-well structure of Ref. 19. Failure to account for carrier screening effects can result in an underestimate of the polarization charge corresponding to a measured quantum-well

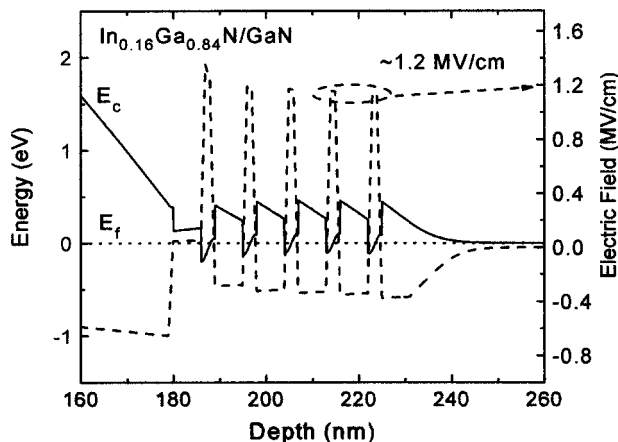


FIG. 5. Simulated band structure and electric field for Ref. 16. The indium content is 16% and the assumed polarization charge density is  $9.0 \times 10^{12} \text{ e/cm}^2$ . The electric field thus deduced is about 1.2 MV/cm.

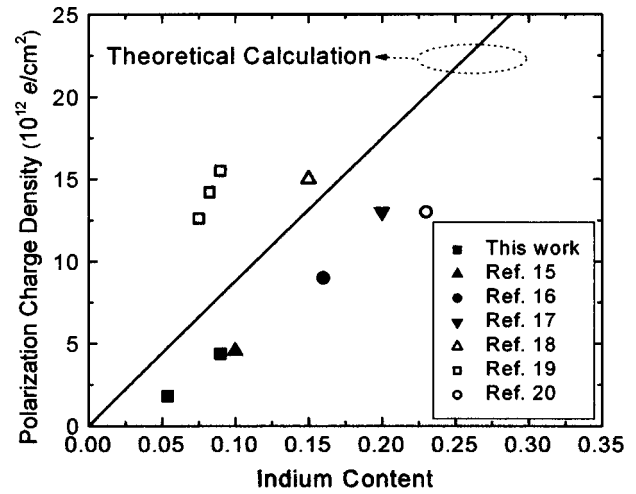


FIG. 6.  $\text{In}_x\text{Ga}_{1-x}\text{N}/\text{GaN}$  polarization charge densities from this work (■), and inferred from Ref. 15 (▲), Ref. 16 (●), Ref. 17 (▼), Ref. 18 (△), Ref. 19 (□) and Ref. 20 (○). Calculated polarization charge densities (Ref. 1) are also shown.

electric field of as much as 20%. By adjusting the polarization charge density until good agreement is achieved between the simulated and optically measured values of the electric field, the polarization charge density can be inferred, as shown in Fig. 6. From Fig. 6, we see that the majority of measurements yield polarization charge densities somewhat lower than those predicted theoretically, but in good agreement with our measured values. Further investigations are needed to determine the origin of the large range of values reported for polarization charge density at the  $\text{In}_x\text{Ga}_{1-x}\text{N}/\text{GaN}$  interface.

#### IV. SUMMARY

In conclusion, we have described in detail the capacitance–voltage profiling method and its modification for the measurement of polarization charge densities and conduction band offsets in the  $\text{In}_{0.054}\text{Ga}_{0.946}\text{N}/\text{GaN}$  and  $\text{In}_{0.09}\text{Ga}_{0.91}\text{N}/\text{GaN}$  heterojunction interfaces. We obtain conduction band offsets of  $0.09 \pm 0.07$  and  $0.22 \pm 0.05$  eV, respectively, which are in good agreement with other reported experimental results. The band offset ratio  $\Delta E_C : \Delta E_V$  is inferred to be 58:42 in this range of In composition. The polarization charge densities at the interfaces are  $(1.80 \pm 0.32) \times 10^{12}$  and  $(4.38 \pm 0.36) \times 10^{12} \text{ e/cm}^2$ , smaller than the theoretical predictions but in good agreement with values inferred from a substantial body of optical data.<sup>25</sup>

#### ACKNOWLEDGMENT

Part of the work was supported by ONR (POLARIS MURI, monitored by Dr. Colin Wood).

<sup>1</sup> S. N. Mohammad and H. Morkoc, *J. Appl. Phys.* **78**, 4200 (1995).

<sup>2</sup> T. Makimoto, K. Kumakura, and N. Kobayashi, *Appl. Phys. Lett.* **83**, 1035 (2003).

<sup>3</sup> S. Nakamura and G. Fasol, *The Blue Laser Diode* (Springer, Berlin, 1997).

- <sup>4</sup>C. Poblenz, T. Mates, M. Craven, S. P. DenBaars, and J. S. Speck, *Appl. Phys. Lett.* **81**, 2767 (2002).
- <sup>5</sup>M. Ershov, H. C. Liu, L. Li, M. Buchanan, Z. R. Wasilewski, and A. K. Jonscher, *IEEE Trans. Electron Devices* **45**, 2196 (1998).
- <sup>6</sup>E. J. Miller, D. M. Schaadt, E. T. Yu, C. Poblenz, C. Elsass, and J. S. Speck, *J. Appl. Phys.* **91**, 9821 (2002).
- <sup>7</sup>E. J. Miller, D. M. Schaadt, E. T. Yu, P. Waltereit, C. Poblenz, and J. S. Speck, *Appl. Phys. Lett.* **82**, 1293 (2003).
- <sup>8</sup>R. Nakasaki, T. Hashizume, and H. Hasegawa, *Physica E (Amsterdam)* **7**, 953 (2000).
- <sup>9</sup>D. Schroder, *Semiconductor Material and Device Characterization*, 2nd ed. (Wiley, Toronto, 1998).
- <sup>10</sup>H. Kroemer, W.-Y. Chien, J. S. Harris, and D. D. Edwall, *Appl. Phys. Lett.* **36**, 295 (1980).
- <sup>11</sup>L. T. Romano, B. S. Krusor, M. D. McCluskey, and D. P. Bour, *Appl. Phys. Lett.* **73**, 1757 (1998).
- <sup>12</sup>C. Wetzel, T. Takeuchi, S. Yamaguchi, H. Katoh, H. Amano, and I. Akasaki, *Appl. Phys. Lett.* **73**, 1994 (1998).
- <sup>13</sup>Ch. Manz, M. Kunzer, H. Obloh, A. Ramakrishnan, and U. Kaufmann, *Appl. Phys. Lett.* **74**, 3993 (1999).
- <sup>14</sup>G. Martin, A. Botchkarev, A. Rockett, and H. Morkoc, *Appl. Phys. Lett.* **68**, 2541 (1996).
- <sup>15</sup>G. Martin, S. Strite, A. Botchkarev, A. Agarwal, A. Rockett, and H. Morkoc, *Appl. Phys. Lett.* **65**, 610 (1994).
- <sup>16</sup>T. Makimoto, K. Kumakura, T. Nishida, and N. Kobayashi, *J. Electron. Mater.* **31**, 313 (2002).
- <sup>17</sup>O. Ambacher *et al.*, *J. Phys.: Condens. Matter* **14**, 3399 (2002).
- <sup>18</sup>S. F. Chichibu *et al.*, *Appl. Phys. Lett.* **73**, 2006 (1998).
- <sup>19</sup>T. Takeuchi *et al.*, *Appl. Phys. Lett.* **73**, 1691 (1998).
- <sup>20</sup>P. Lefebvre *et al.*, *Appl. Phys. Lett.* **78**, 1252 (2001).
- <sup>21</sup>Y. D. Jho, J. S. Yahng, E. Oh, and D. S. Kim, *Appl. Phys. Lett.* **79**, 1130 (2001).
- <sup>22</sup>F. Renner, P. Kiesel, G. H. Döhler, M. Kneissl, C. G. Van de Walle, and N. M. Johnson, *Appl. Phys. Lett.* **81**, 490 (2002).
- <sup>23</sup>C. Y. Lai, T. M. Hsu, W.-H. Chang, and K.-U. Tseng, *J. Appl. Phys.* **91**, 531 (2002).
- <sup>24</sup>G. L. Snider, computer program 1D Poisson/Schrödinger: A band diagram calculator, University of Notre Dame, Notre Dame, IN, 1995.
- <sup>25</sup>W. H. Press, S. A. Teukolsky, W. T. Vetterling, and B. P. Flannery, *Numerical Recipes in Fortran: The Art of Scientific Computing*, 2nd ed. (Cambridge University Press, Cambridge, U.K., 1992).